Toroidal self-consistent modeling of drift kinetic effects on the resistive wall mode

Yueqiang Liu,[1,a)] M. S. Chu,[2] I. T. Chapman,[1] and T. C. Hender[1]
[1]*Euratom/UKAEA Fusion Association, Culham Science Centre, Abingdon, OX14 3DB, United Kingdom*
[2]*General Atomics, San Diego, California 29186, USA*

(Received 15 August 2008; accepted 6 October 2008; published online 12 November 2008)

A self-consistent kinetic model is developed to study the stability of the resistive wall mode in toroidal plasmas. This model is compared with other models based on perturbative approaches. The degree of the kinetic modification to the stability of the mode depends on the plasma configurations. Both stabilizing and destabilizing kinetic effects are observed. The nonperturbative approach, with a self-consistent inclusion of the eigenfunctions and the eigenvalues of the resistive wall mode, normally finds less stabilization than the perturbative approach. © *2008 American Institute of Physics*. [DOI: 10.1063/1.3008045]

I. INTRODUCTION

It is well known that the pressure driven resistive wall mode (RWM) instability may pose an operational limit to steady state advanced tokamak scenarios.[1] The $n=1$ RWM has been predicted to be unstable in the ITER[2] steady state scenario-4, just beyond the target plasma pressure, unless a sufficiently fast plasma rotation, or a magnetic feedback system, is available.[3]

While the feedback stabilization of the RWM has been well understood in theory and demonstrated in several tokamaks and RFP devices, the physics of rotational stabilization of the RWM is not completely resolved, partly because new experimental evidence[4,5] contradicts previous theories based on the magnetohydrodynamic (MHD) description of the mode.

Earlier theories of the RWM damping rely either on the ideal[6] or resistive[7] MHD descriptions. In the ideal MHD model, either sound wave[6,8] or Alfvén continuum[9,10] resonance is suggested as the main energy-releasing channel for the damping of RWM in the presence of a rather fast toroidal plasma rotation. The rotation frequency required to make the mode marginally stable was predicted to be a few percent of the Alfvén frequency. The same range of rotation frequency is predicted for the RWM stability in ITER,[3] which is likely to be only marginally achievable due to the large plasma volume and the constraints on the tangential neutral beam heating capability. The resistive model is based on the coupling to the inertial layers inside the plasma, which gives rise to resistive or viscous energy dissipation. This model predicts a different scaling of the critical rotation frequency for mode stability.[7,11]

A strong viscous term simulating the parallel sound wave damping is introduced into the MHD equations,[12] which sometimes leads to a reasonable prediction of the critical rotation speed measured in experiments.[13–15] A more physics-based damping model, including the mode resonance with bounce motions of thermal ions of the plasma, is suggested in Ref. 16 and numerically implemented in the MARS-F code.[17,14] Since the kinetic terms are derived for a large aspect ratio plasma, this model is labeled the semi-kinetic damping model, which nevertheless predicts rather well the RWM stability thresholds for fast rotating plasmas.[13–15] In some cases, even at low plasma rotation (much less than 1% of the Alfvén speed), the semi-kinetic model predicts a rotation threshold comparable with the experimental value.[4]

Recently, a new kinetic damping mechanism is suggested for RWM suppression[18,19] in the regime of very slow plasma rotation, or even in the absence of rotation. Resonance of the mode with the magnetic precession drifts of trapped thermal ions and electrons is proposed as the main energy dissipation channel. This model predicts that the RWM growth rate is significantly reduced and the mode is almost fully suppressed, for a plasma close to the ITER steady state scenario. In Ref. 18, a nonperturbative treatment of the kinetic terms is carried out, but for a significantly simplified assumption of the plasma configuration. In Ref. 19, a realistic toroidal plasma is used, with the kinetic terms included in the MHD calculations in a perturbative manner. A stabilizing contribution of alpha particles is also included in Ref. 19, but is neglected in this work.

The perturbative approach normally uses the eigenfunction of the ideal kink mode, computed by an ideal MHD code, as the input to further compute the kinetic energy δW_k. The stability of the RWM is then determined by the following extended RWM dispersion relation,[20,12] derived from the kinetic MHD energy principle

$$\gamma\tau_w^* \simeq -\frac{\delta W_\infty + \delta W_k}{\delta W_b + \delta W_k}, \tag{1}$$

where τ_w^* is the typical wall eddy current decay time, and δW_∞ and δW_b are the fluid potential energies without and with a conducting wall, respectively. The fluid energy includes both the plasma and the vacuum contributions.

This dispersion relation, subject to certain normalization of the energy terms, generally describes the RWM stability well, without taking into account the plasma inertia effect, which can often be neglected as long as the resistive wall time is orders of magnitude larger than the Alfvén time.

a)Electronic mail: yueqiang.liu@ukaea.org.uk.

In this work, we describe a nonperturbative approach for the inclusion of the drift kinetic terms into the MHD equations, in a general toroidal geometry. We compare the kinetic effects on the stability of the RWM between the perturbative and nonperturbative approaches. Formally, the latter differs from the former in two essential aspects. (1) The nonperturbative approach allows a self-consistent modification of the eigenfunction of the RWM, due to the presence of the kinetic terms. (2) The growth rate (complex frequency) of the RWM enters self-consistently into the kinetic integrals, which makes the eventual eigenvalue problem nonlinear.

The next section gives a detailed description of the nonperturbative formulation, which is the basis of the recently developed MARS-K code. Section III reports the benchmark results of MARS-K against both analytical theory and other kinetic codes. Computational results for an analytical, elongated toroidal plasma are given in Sec. IV. Section V summarizes the paper.

II. TOROIDAL SELF-CONSISTENT KINETIC MODEL

We consider the single-fluid MHD description of plasmas with a toroidal flow. The core equations, where the kinetic terms are involved, are written in the Eulerian frame

$$(\gamma + in\Omega)\boldsymbol{\xi} = \mathbf{v} + (\boldsymbol{\xi}\cdot\nabla\Omega)R^2\nabla\phi, \tag{2}$$

$$\rho(\gamma + in\Omega)\mathbf{v} = -\nabla\cdot\mathbf{p} + \mathbf{j}\times\mathbf{B} + \mathbf{J}\times\mathbf{Q} - \rho[2\Omega\hat{\mathbf{Z}}\times\mathbf{v} + (\mathbf{v}\cdot\nabla\Omega)R^2\nabla\phi], \tag{3}$$

$$(\gamma + in\Omega)\mathbf{Q} = \nabla\times(\mathbf{v}\times\mathbf{B}) + (\mathbf{Q}\cdot\nabla\Omega)R^2\nabla\phi, \tag{4}$$

$$(\gamma + in\Omega)p = -\mathbf{v}\cdot\nabla P, \tag{5}$$

$$\mathbf{j} = \nabla\times\mathbf{Q}, \tag{6}$$

$$\mathbf{p} = p\mathbf{I} + p_{\parallel}\hat{\mathbf{b}}\hat{\mathbf{b}} + p_{\perp}(\mathbf{I} - \hat{\mathbf{b}}\hat{\mathbf{b}}), \tag{7}$$

where the variables $\boldsymbol{\xi}$, $\mathbf{v}$, $\mathbf{Q}$, $\mathbf{j}$, $\mathbf{p}$ represent the plasma displacement, perturbed velocity, magnetic field, current, and pressure tensor, respectively. ρ is the unperturbed plasma density. The linear problem is formulated as an eigenvalue problem, with γ being the eigenvalue, which is corrected by a Doppler shift $in\Omega$, with n being the toroidal mode number, Ω the plasma rotation frequency along the toroidal angle ϕ. The equilibrium field, current, and pressure are denoted by $\mathbf{B}$, $\mathbf{J}$, $\mathbf{P}$, respectively. R is the plasma major radius, $\hat{\mathbf{Z}}$ the unit vector in the vertical direction, and $\mathbf{I}$ the unit tensor. A conventional unit system is assumed with the vacuum permeability $\mu_0 = 1$.

The kinetic terms enter into the MHD equations via the perturbed kinetic pressure tensors shown in Eq. (7), where p is the scalar fluid pressure perturbation, $p_{\parallel}(\boldsymbol{\xi}_{\perp})$ and $p_{\perp}(\boldsymbol{\xi}_{\perp})$ are the parallel and perpendicular components of the kinetic pressure perturbations, respectively, and $\hat{\mathbf{b}} = \mathbf{B}/B$, $B = |\mathbf{B}|$. The full pressure tensor $\mathbf{p}$ is self-consistently included into the MHD formulation via the momentum equation (3).

The remaining terms in the right-hand side (RHS) of Eqs. (2)–(6) are the standard MHD operators for an ideal plasma, and the terms associated with shear flow. We ignore a term $\rho_1(\mathbf{V}_0\cdot\nabla)\mathbf{V}_0$ of quadratic order in Ω ($\mathbf{V}_0 = R\Omega\hat{\phi}$), which allows us to exclude the equation for the perturbed plasma density ρ_1 from consideration.

Note that the ordinary $5/3P\nabla\cdot\mathbf{v}$ term is also dropped from Eq. (5) for the perturbed fluid pressure. This term is effectively replaced by the kinetic pressure tensors.

Equations (2)–(7) do not represent the full set of equations that MARS-K solves. For the RWM study, a set of vacuum equations for the magnetic field $\mathbf{Q}$, an equation for the resistive wall in the thin-shell approximation and an equation for the active feedback coils, are also included and solved together with Eqs. (2)–(7). These aspects are described in Ref. 17 and will not be discussed further in this paper. In addition, other kinetic damping models, such as the parallel sound wave damping or the semi-kinetic damping,[3] are also included in the MARS-K code, but are not described here. The resistive term in the Ohm's law is also dropped.

The perturbed kinetic pressure tensors are calculated following basically the procedures described in Refs. 21 and 22. We list here some key steps which lead to forms for $p_{\parallel}$ and $p_{\perp}$, which can be conveniently merged into the MHD formalism.

We start with

$$p_{\parallel}e^{-i\omega t + in\phi} = \sum_{e,i}\int d\Gamma M v_{\parallel}^2 f_L^1, \tag{8}$$

$$p_{\perp}e^{-i\omega t + in\phi} = \sum_{e,i}\int d\Gamma \frac{1}{2} M v_{\perp}^2 f_L^1, \tag{9}$$

where an $\exp(-i\omega t + in\phi)$ dependence is explicitly assumed for the perturbation, with the mode frequency $\omega \equiv i\gamma$. The integral is carried out over the particle velocity space Γ. M is the particle mass, $v_{\parallel}$ and $v_{\perp}$ are, respectively, the parallel and perpendicular (to the equilibrium magnetic field) velocities of particle bounce motion, and f_L^1 is the perturbed distribution function defined in the Lagrangian frame, and satisfies

$$\frac{df_L^1}{dt} = f_{\epsilon}^0\frac{\partial H^1}{\partial t} - f_{P_\phi}^0\frac{\partial H^1}{\partial\phi} - \nu_{\mathrm{eff}}f_L^1, \tag{10}$$

where $f^0(\psi,\varepsilon)$ is the equilibrium particle distribution function, which we assume to be Maxwellian for thermal ions and electrons. ψ is the poloidal flux, $0 < \psi < \psi_a$, and $\varepsilon = \varepsilon_k + Ze\Phi = Mv^2/2 + Ze\Phi$ is the particle total energy, with Z being the charge number and Φ the equilibrium electrostatic potential. The toroidal canonical momentum P_ϕ is defined as

$$P_\phi = MR^2\dot{\phi} - Ze\psi.$$

The last term in the RHS of Eq. (10) represents a simple linear collision operator, with coefficient ν_{eff}.

The quantity H^1 denotes the perturbed Lagrangian $H^1 = -\varepsilon_k H_L\exp(-i\omega t + in\phi)$, with

$$H_L = \frac{1}{\epsilon_k}[Mv_{\parallel}^2\vec{\kappa}\cdot\boldsymbol{\xi}_{\perp} + \mu(Q_{L\parallel} + \nabla B\cdot\boldsymbol{\xi}_{\perp})], \tag{11}$$

where $\vec{\kappa} = (\hat{\mathbf{b}}\cdot\nabla)\hat{\mathbf{b}}$ is the magnetic curvature, and $\mu = Mv_{\perp}^2/2B$ the particle magnetic moment. Note that although

it is possible to replace $Q_{L\|}$ in Eq. (11) by $\boldsymbol{\xi}_\perp$ using $\mathbf{Q}_L = \nabla\times(\boldsymbol{\xi}_\perp\times\mathbf{B})$, we keep $Q_{L\|}$ in the calculations for H_L, in order to avoid the radial derivatives of $\boldsymbol{\xi}_\perp$ in the final expressions for $p_\|$ and $p_\perp$.

The quantity H_L can be symbolically written as

$$H_L = \sum_u C_u(s,\chi,\Lambda)X^u(s,\chi), \tag{12}$$

where C_u are coefficients depending on the equilibrium quantities and the particle pitch angle parameter $\Lambda \equiv B_0\mu/\varepsilon_k$ (B_0 can be defined as the on-axis field amplitude). These coefficients are easily derived for a given curvilinear coordinate system (s,χ,ϕ), where s labels the flux surface and χ is a generalized poloidal angle. The variables X^u denote the two components perpendicular to $\mathbf{B}$ of the solution vector $\boldsymbol{\xi}_\perp$, and the parallel component of $\mathbf{Q}_L$. These variables are further decomposed in Fourier harmonics along the poloidal angle

$$X^u(s,\chi) = \sum_m X^u_m(s)e^{im\chi}.$$

A few lengthy, but straightforward steps, i.e.,

(1) substituting the form (12) for the particle Lagrangian into Eq. (10),
(2) integrating over time t, starting from $t=-\infty$, and assuming an unstable perturbation $\mathrm{Re}(-i\omega)>0$,
(3) utilizing the standard technique of decomposing the integrand in time into periodic and secular parts, and
(4) Fourier decomposing the periodic part in particle bounce orbit,

lead to the final expression for f_L^1

$$f_L^1 = -f_\epsilon^0\epsilon_k e^{-i\omega t+in\phi}\sum_{m,l,u} X^u_m H^u_{ml}\lambda_{ml}e^{-in\tilde{\phi}(t)+im\langle\dot{\chi}\rangle t+il\omega_b t}, \tag{13}$$

where $\tilde{\phi}(t)=\phi(t)-\langle\dot{\phi}\rangle t$, $\langle\cdot\rangle$ denotes the average over particle bounce period, ω_b is the bounce frequency, and l is the harmonic number in the bounce orbit expansion. The factor H^u_{ml} is defined as

$$H^u_{ml} = \frac{\omega_b}{2\pi}\oint C^u(\chi(\tau))e^{im\tilde{\chi}(\tau)+in\tilde{\phi}(\tau)-il\omega_b\tau}d\tau, \tag{14}$$

with $\tilde{\chi}(\tau)=\chi(\tau)-\langle\dot{\chi}\rangle\tau$.

The factor λ_{ml} in Eq. (13) represents the mode-particle resonance operator

$$\lambda_{ml} = \frac{n[\omega_{*N}+(\hat{\epsilon}_k-3/2)\omega_{*T}+\omega_E]-\omega}{m\langle\dot{\chi}\rangle+n\langle\dot{\phi}\rangle+l\omega_b-i\nu_{\mathrm{eff}}-\omega}$$
$$= \frac{n[\omega_{*N}+(\hat{\epsilon}_k-3/2)\omega_{*T}+\omega_E]-\omega}{n\omega_d+[\alpha(m+nq)+l]\omega_b-i\nu_{\mathrm{eff}}-\omega} = \lambda_{\alpha m+l}, \tag{15}$$

where ω_{*N} and ω_{*T} are the diamagnetic drift frequencies due to the density and temperature gradients, respectively. ω_E is the $\mathbf{E}\times\mathbf{B}$ drift due to the equilibrium electrostatic potential. $\omega_d=\langle\dot{\phi}\rangle$ is the bounce-orbit-averaged toroidal precession drift frequency of particles, including the ω_E drift. $\hat{\varepsilon}_k=\varepsilon_k/T$ is the particle kinetic energy normalized by the temperature. $\alpha=1$ for passing particles, and $\alpha=0$ for trapped particles.

We point out that in the integration over the particle bounce orbit in the above procedures, we have assumed that the bounce orbit is not affected by the magnetic drift motion. In other words, we have neglected the effect of finite radial excursion width of particles across the magnetic surfaces.

Equation (15) shows that both particle bounce and magnetic precession drift resonances are included in this formulation. However, these contributions depend on the plasma rotation frequency and the particle species, as well as the particle trapping. Normally, bounce resonance occurs dominantly at relatively fast plasma rotation, $\omega_E\sim\omega_b$. Some contribution can also come from slow plasma rotation in the plasma edge region, where ω_b is small. Both passing and trapped ions contribute. The electrons' contribution to bounce resonance damping is negligible. The precessional resonance occurs at slow plasma rotation, $\omega_E\lesssim\omega_*$. Both ions and electrons contribute. The contribution of passing particles is small because the bounce frequency always prevails over the precession frequency, except in narrow regions around the rational surfaces. The contribution of trapped particles ($\alpha=0$) comes mainly from the $l=0$ bounce harmonic at slow rotation.

We also notice that the mode eigenvalue γ enters into the resonance operator (15) via $\omega=i\gamma$. This is another important aspect of the self-consistency of the kinetic formulation. However, this makes the eigenvalue problem nonlinear, which requires an outer iterative loop for solving the eventual eigenvalue problem.

Knowing the perturbed distribution function f_L^1, it is straightforward to compute the perturbed kinetic pressures by substituting Eq. (13) into Eqs. (8) and (9). However, for the numerical implementation, it is more convenient to calculate directly the poloidal Fourier harmonic of $p_\|$ and $p_\perp$, normalized by the Jacobian J of the curvilinear coordinate mapping.

After decomposing the velocity space integration $\int\cdot d\Gamma$ in Eqs. (8) and (9) into the integration over the particle energy and pitch angle $\int\int\cdot d\hat{\varepsilon}_k d\Lambda$, and projecting the perturbed pressures into the Fourier space, we obtain

$$(Jp_\|)_k = \frac{1}{\sqrt{\pi}}\sum_{e,i}\sum_{m,l,u}\frac{P_{e,i}}{B_0}\int d\Lambda I_{ml}H^u_{ml}G^\|_{kml}X^u_m, \tag{16}$$

$$(Jp_\perp)_k = \frac{1}{\sqrt{\pi}}\sum_{e,i}\sum_{m,l,u}\frac{P_{e,i}}{B_0}\int d\Lambda I_{ml}H^u_{ml}G^\perp_{kml}X^u_m, \tag{17}$$

where the energy factor I is obtained by integrating the resonance operator over the particle energy

$$I_{ml} = \sum_\sigma\int_0^\infty d\hat{\epsilon}_k\hat{\epsilon}_k^{5/2}e^{-\hat{\epsilon}_k}\lambda_{ml}, \tag{18}$$

where $\sigma=\mathrm{sign}(v_\|)$. If we neglect the particle energy dependence of ν_{eff}, this integral can be performed analytically, with the results expressed in terms of the standard plasma dispersion function.

The geometrical factor G in Eqs. (16) and (17) is obtained after the Fourier projection, resulting in

$$G_{kml}^{\parallel} = \frac{1}{2\pi}\int_{\chi_L}^{\chi_U} JB\sqrt{1-\Lambda/h}\, e^{i[\alpha(m+nq)+l]\omega_b t(\chi)-in\phi(\chi)-ik\chi} d\chi, \quad (19)$$

$$G_{kml}^{\perp} = \frac{1}{2\pi}\int_{\chi_L}^{\chi_U} \frac{JB\Lambda/(2h)}{\sqrt{1-\Lambda/h}} e^{i[\alpha(m+nq)+l]\omega_b t(\chi)-in\phi(\chi)-ik\chi} d\chi, \quad (20)$$

where $h=B_0/B$, and χ_L and χ_U the lower and upper reflecting points for trapped particles, respectively. For passing particles, the integrals are taken from $-\pi$ to π.

The integrands for both the G-factor (20) and the H-factor (14) are singular at the turning points for trapped particles. In the numerical implementation, these singularities are extracted analytically. Another singularity can occur in the I-factor (18), when the final integrals (16) and (17) over pitch angle Λ are performed. A semi-analytic approach is adopted where the singular part is numerically extracted and integrated on a very dense and nonuniform Λ-grid.

It can be shown that the perturbed kinetic pressures derived above yield the same kinetic energy as in Ref. 19:

$$\begin{aligned}\delta W_K &= \sum_{e,i}\frac{1}{2}\int d^3x \int d\Gamma(-f_\epsilon^0)\sum_l \hat{\lambda}_l |\langle e^{-il\omega_b t}\tilde{H}(t)\rangle|^2 \\ &= \frac{\sqrt{\pi}}{2}\frac{\nu}{B_0}\sum_{e,i}\int d\psi P_{e,i}\int d\hat{\epsilon}_k \sum_l \sum_\sigma \hat{\epsilon}_k^{5/2} \\ &\quad \times e^{-\hat{\epsilon}_k}\hat{\lambda}_l \int d\Lambda \hat{\tau}_b |\langle e^{-il\omega_b t+in\tilde{\phi}(t)} H_L\rangle|^2, \end{aligned} \quad (21)$$

where

$$\tilde{H}(t) = \epsilon_k H_L e^{in\tilde{\phi}(t)} = \epsilon_k H_L e^{in\phi - in\alpha q\omega_b t},$$

$$\hat{\lambda}_l = \frac{n[\omega_{*N} + (\hat{\epsilon}_k - 3/2)\omega_{*T} + \omega_E] - \omega}{n\omega_d + (\alpha nq + l)\omega_b - i\nu_{\text{eff}} - \omega},$$

and $\nu=1/2$ for trapped particles, $\nu=1$ for passing particles. $\hat{\tau}_b$ is the bounce period normalized by a factor $\sqrt{M/2\varepsilon_k}$.

We summarize the self-consistent kinetic formulation by listing the effects that have been neglected:

- the anisotropy of equilibrium pressure
- the perturbed electrostatic potential
- the radial excursion of particle trajectory
- the finite Larmor radius corrections to the particle orbit.

These effects normally are not important for the RWM. Some of them are crucial to study the kinetic effects on other MHD modes, such as the internal kink mode. Although the formulation is presented for thermal particles, for which a Maxwellian distribution function over the particle energy is assumed. It is relatively easy to extend it to include, for instance, fast ions contribution or anisotropic distribution functions. Largely only the numerator of the resonance operator λ_{ml} has to be rederived.

III. NUMERICAL TEST RESULTS

In this work, we are mostly interested in the RWM damping at slow plasma rotation; hence, all the numerical calculations have been performed with inclusion of the precession drift resonance effect only. The benchmark of the newly developed MARS-K code is performed mostly for the perturbative approach, where other codes based on perturbative formalisms are available.

We emphasize that such tests cover the major part of the numerical implementation associated with the self-consistent approach, since the same subroutines are used to evaluate the kinetic integrals, for both perturbative and nonperturbative options in the MARS-K code. The fluid portion of the code, which consists mainly of the underlying MARS-F[17] code, has been previously extensively benchmarked.

In addition, a separate subroutine is designed to compute the perturbed kinetic pressures at the Kruskal–Oberman high-frequency limit, where only the fluidlike terms (kinetic integrals are performed analytically in this limit) are present. Internal tests within the same code have been performed to make sure that the numerically implemented kinetic integrals converge to the fluid terms at high frequency.

A. Test equilibrium

We consider the analytical Solov'ev equilibrium[23] with constant toroidal magnetic field F, and linear pressure profile in the poloidal flux ψ:

$$P(\psi) = -\frac{1+\kappa^2}{\kappa R_0^3 q_0}\psi, \quad F(\psi) = 1, \quad (22)$$

where κ is the plasma elongation, q_0 is the safety factor at the plasma center.

The analytical solution of the Grad–Shafranov equation is

$$\psi = \frac{\kappa}{2R_0^3 q_0}\left(\frac{R^2Z^2}{\kappa^2} + \frac{1}{4}(R^2 - R_0^2)^2 - a^2R_0^2\right), \quad (23)$$

with the plasma boundary specified by

$$R = R_0(1 + 2\epsilon_a \cos\theta)^{1/2},$$

$$Z = \frac{R_0\epsilon_a\kappa \sin\theta}{(1+2\epsilon_a\cos\theta)^{1/2}},$$

with $\varepsilon_a \equiv a/R_0$. Hence, the equilibrium is fully specified by three parameters $\{\varepsilon_a, \kappa, q_0\}$.

For the numerical test, we choose a circularlike equilibrium with

$$\epsilon_a = 0.2, \quad \kappa = 1.0, \quad q_0 = 1.2. \quad (24)$$

No $n=1$ rational surfaces exist inside the plasma ($q_{\text{edge}}=1.414$). The normalized pressure is $\beta_N=3.126$. The marginal ideal wall position for the $n=1$ ideal external kink stability is $1.274a$.

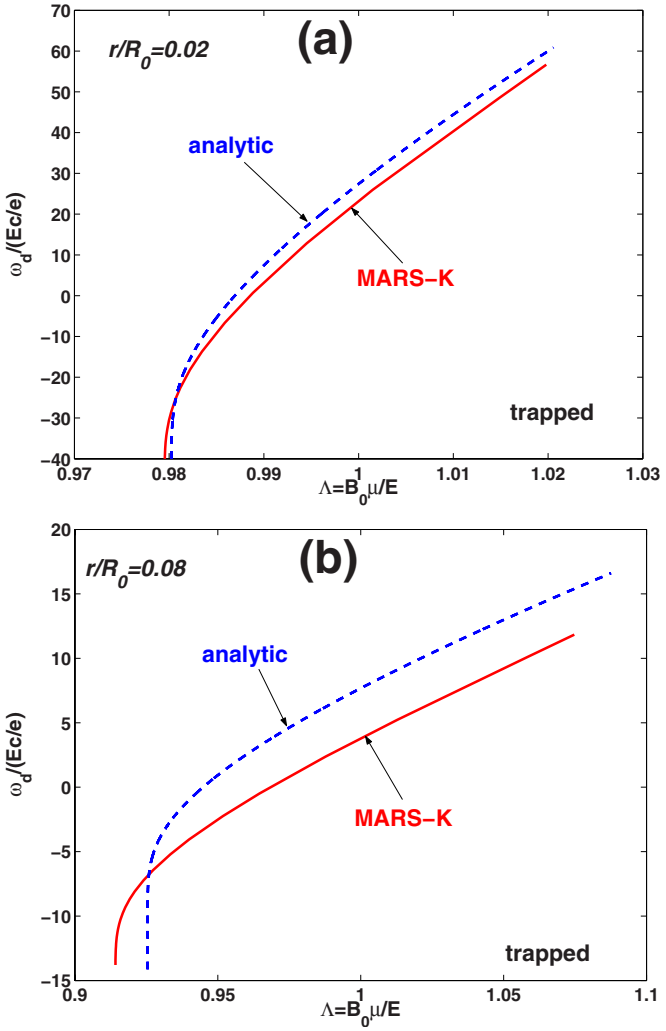

FIG. 1. (Color online) Comparison of the processional drift frequency of trapped particles computed by MARS-K, with analytical expressions from a large aspect ratio approximation. Numerical results are obtained for the circularlike Solov'ev plasma described by Eq. (23) with parameters (24) at aspect ratio (a) $r/R_0=0.02$ and (b) $r/R_0=0.08$. Analytical results correspond to the same aspect ratios, but for a circular flux surface with prescribed magnetic fields.

B. Comparison with analytical results

Figures 1(a) and 1(b) compare the bounce-orbit-averaged precessional drift frequency ω_d computed by MARS-K, with that from a large aspect ratio analytical calculation,[24] where a prescribed magnetic field of the type $B=B_0(1-\varepsilon_r\cos\theta)$ is assumed for the particle orbit calculation

$$\omega_d^{\text{ana}}=\frac{2cq\epsilon_k\Lambda}{eR_0B_0r}\left[(2s+1)\frac{E(k_t)}{K(k_t)}+2s(k_t^2-1)-\frac{1}{2}\right], \qquad (25)$$

where e is the particle charge, $s=rq'/q$ the magnetic shear. $K(k)=\int_0^{\pi/2}d\varphi/\sqrt{1-k^2\sin^2\varphi}$, and $E(k)=\int_0^{\pi/2}d\varphi\sqrt{1-k^2\sin^2\varphi}$ are the complete elliptic integrals of the first and second kind, respectively. $k_t=\sqrt{(1-\Lambda+\Lambda\varepsilon_r)/2\Lambda\varepsilon_r}$ with $\varepsilon_r=r/R_0$ the inverse aspect ratio. The safety factor q is taken from the Solov'ev equilibrium (23) with parameters (24).

The drift frequency in the figures is normalized by the particle energy $E\equiv\varepsilon_k$ and charge e, $\omega_d/(Ec/e)$. Shown is the dependence on the particle pitch angle Λ. Figure 1(a) shows the comparison for $\varepsilon_r=0.02$, corresponding to a minor radius of $r=0.1$. Because of the smallness of the toroidal correction in this case, the numerically computed drift frequency agrees well with the theory. At a larger $\varepsilon_r=0.08$, corresponding to a minor radius of $r=0.4$, the computed drift frequency shows a significant shift. This is partly due to the higher order terms in ε_r in the toroidal calculations, and partly due to a correction term from the finite equilibrium pressure,[25] which is taken into account consistently in the toroidal calculations, but neglected in the analytic formula.

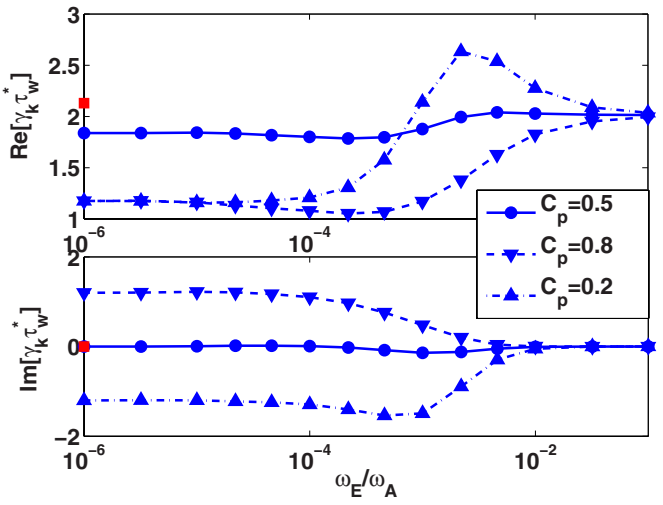

FIG. 2. (Color online) Eigenvalue of the RWM, modified by the kinetic resonances, vs the frequency of a uniformly rotating plasma. The circularlike Solov'ev plasma, described by Eq. (23) with parameters (24), is used. Various ratios of ion-electron pressures are assumed. The fluid growth rate (single square) is also plotted for comparison. The wall position is at $r_w=1.15a$. An ion gyrofrequency at the plasma center $\omega_{ci}=100\omega_A$ is assumed.

Figure 2 scans the kinetically modified growth rate of the RWM as a function of the plasma rotation frequency ω_E, following the perturbative approach. Since a uniform rotation induces effectively the mode frequency of the same magnitude due to the Doppler shift, the results can also be interpreted as a scan over the mode frequency ω. Three types of plasmas are studied, with different ion-electron temperature ratios, corresponding to $C_p=0.5$, 0.8, and 0.2, where $C_p=T_i/(T_i+T_e)$. Note that at very high rotation frequency, the kinetic effects do not come from the precession drift resonances anymore, but rather act as the high frequency term of the Kruskal–Oberman type.[26] Nevertheless, a scan over the full frequency range is useful for benchmark purposes. We make a few interesting observations. (1) When the ion and electron temperature is not equal ($C_p\neq0.5$), precession drift resonances introduce a finite mode frequency even in the absence of the plasma rotation. (2) For the given direction of the plasma rotation (along the ω_{*i} direction), higher ion temperature ($C_p>0.5$) generally leads to more stabilization by the kinetic effects, than the higher electron temperature ($C_p<0.5$). (3) In fact, for $C_p=0.2$ for a certain interval of rotation frequency, the drift resonances destabilize the RWM compared with the static fluid description (denoted by a single square). All these features, as well as the shape of the curves shown in Fig. 2, qualitatively agree well with an analytical calculation in Ref. 27 (see Fig. 10 there).

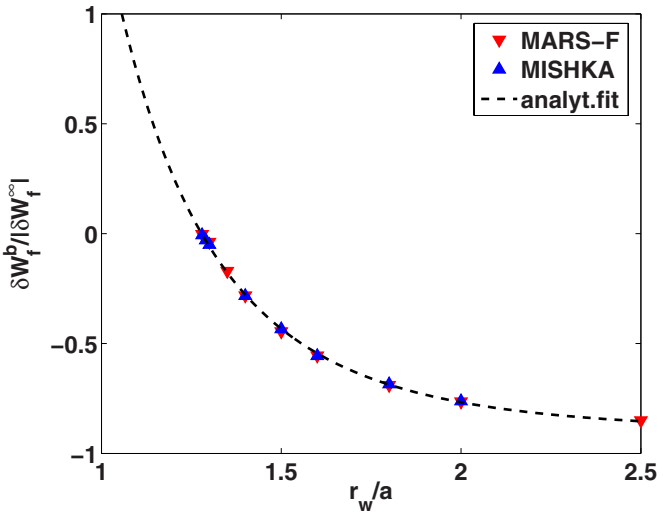

FIG. 3. (Color online) Comparison of the fluid potential energy δW_f^b of the ideal kink mode computed by the MARS-K and MISHKA codes, vs the radial position of an ideal wall. The energy is normalized by the magnitude of the no-wall kink energy δW_f^∞. A circularlike Solov'ev equilibrium, described by Eq. (23) with parameters (24), is used.

C. Comparison with results from MISHKA plus HAGIS codes

Another set of codes has recently been used to study the kinetic effects on RWM stability,[28] following the perturbative approach, where the eigenfunction of the ideal kink mode is computed using the MHD stability code MISHKA,[29] and the kinetic resonances (δW_k) are computed using the HAGIS code,[30] which follows the true guiding center orbit of an assembly of particles. The latter makes the kinetic calculations (within the perturbative approach) more accurately than codes like MARS-K.

We have compared the fluid energy computed by MARS-K and MISHKA, and found very good agreement, as shown in Fig. 3. Only the unstable modes ($\delta W_f^b < 0$) are computed by both codes. The potential energy for the stable modes is extracted from the unstable ones using an analytical fit.

Figures 4(a) and 4(b) compare δW_k computed by MARS-K (perturbatively) and by MISHKA plus HAGIS, for the same Solov'ev equilibrium. The kinetic energy, which comes from the precession drift resonances of thermal trapped ions and electrons of equal temperature, is normalized by the fluid potential energy of the ideal kink mode with the wall at infinity. Both codes scan a wide range of the plasma rotation frequency with a uniform rotation profile, which is equivalent to scanning the mode frequency. An excellent agreement is obtained between the two codes, which also indicates that for this plasma, the approximation made in the MARS-K formulation concerning particle orbit (vanishing banana width of trapped ions) is adequate.

Figures 5(a) and 5(b) compare the two codes in terms of the growth rate of the RWM versus the plasma rotation frequency. The growth rate is calculated using the fluid energy shown in Fig. 3, the kinetic energy from Fig. 4 and utilizing the RWM dispersion relation (1). A wall position of $r_w = 1.15a$ is chosen. Comparing with the fluid growth rate (indicated by the dashed line), only a slight stabilization of the RWM is achieved by the drift kinetic effects.

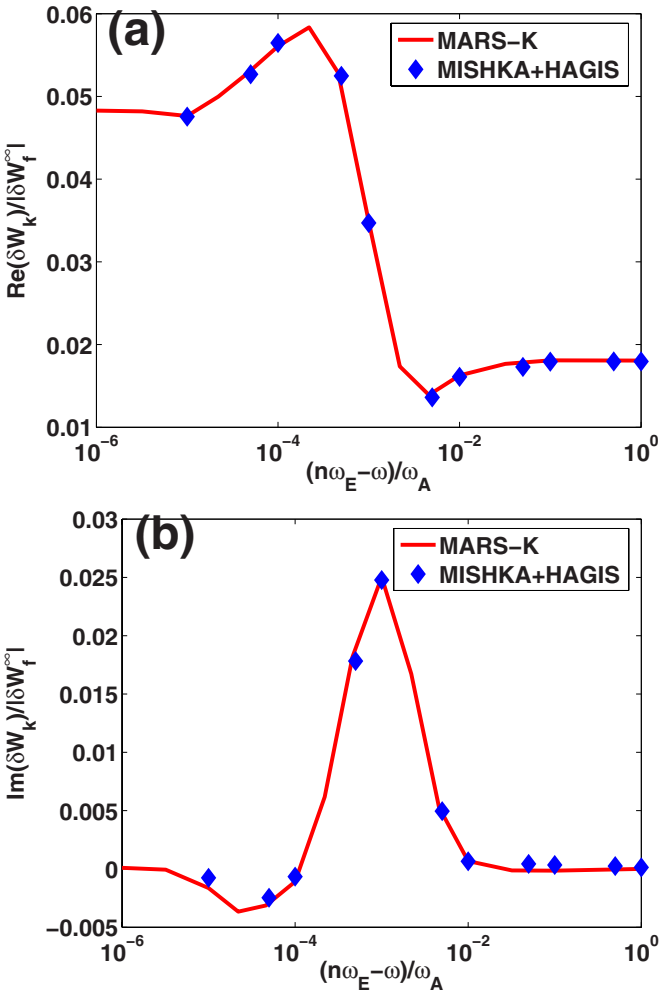

FIG. 4. (Color online) The (a) real and (b) imaginary parts of the drift kinetic energy, computed by the MARS-K and the HAGIS codes, respectively, vs the frequency of a uniformly rotating plasma, for a circularlike Solov'ev equilibrium described by Eq. (23) with parameters (24). The precessional drift resonances from both trapped thermal ions and electrons, with equal equilibrium temperatures, are included. An ion gyrofrequency at the plasma center $\omega_{ci} = 121\omega_A$ is assumed.

Figures 6(a) and 6(b) compare the growth rates of the RWM versus the wall minor radius, for a chosen mode frequency, $\omega = 10^{-3}\omega_A$. Two cases are considered; the first case (dashed lines) includes the drift kinetic contribution from the ions only, while the second case (dot-dashed) includes both ions and electrons with an equal temperature. In both cases, good agreement is obtained between the perturbative MARS-K and HAGIS results. We also note that both codes predict a destabilizing effect of the kinetic contribution from trapped electrons. This also confirms the observation made in Fig. 2.

IV. RESULTS FOR A SHAPED TOROIDAL PLASMA

A toroidal plasma is specified by the Solov'ev equilibrium (23) with

$$\epsilon_a = 0.33, \quad \kappa = 1.6, \quad q_0 = 1.9. \tag{26}$$

This choice of q_0 allows two rational surfaces, $q=2$ and 3, inside the plasma ($q_{\mathrm{edge}} = 3.263$). Even though the instability

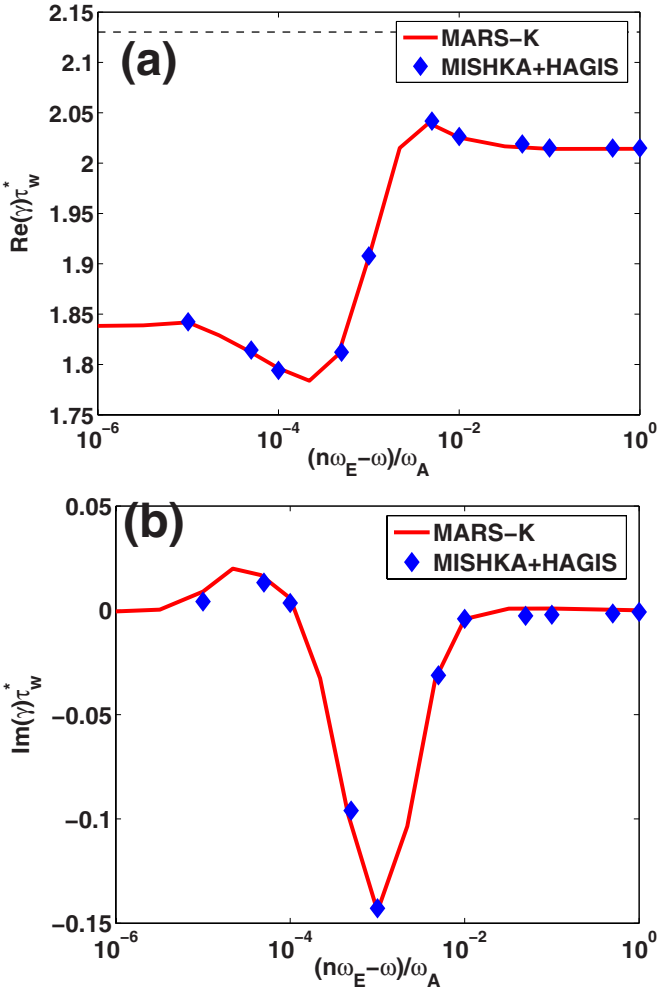

FIG. 5. (Color online) The (a) real and (b) imaginary parts of the kinetically modified RWM growth rate, computed by the MARS-K and the HAGIS codes, respectively, versus the frequency of a uniformly rotating plasma, for a circularlike Solov'ev equilibrium described by Eq. (23) with parameters (24). The precessional drift resonances from both trapped thermal ions and electrons, with equal equilibrium temperatures, are included. The wall position is at $r_w=1.15a$. An ion gyrofrequency at the plasma center $\omega_{ci}=121\omega_A$ is assumed.

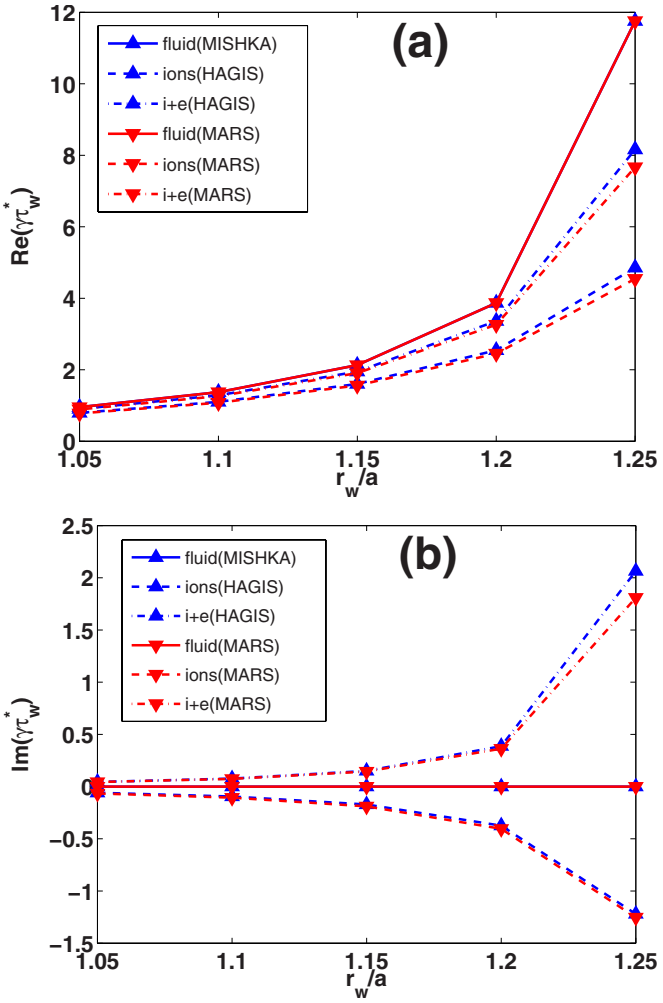

FIG. 6. (Color online) The (a) real and (b) imaginary parts of the kinetically modified RWM growth rate, computed by the MARS-K and the HAGIS codes, respectively, vs the wall radius r_w, for a circularlike Solov'ev equilibrium described by Eq. (23) with parameters (24). The precessional drift resonances from trapped thermal ions only (dashed), or from both ions and electrons (dot-dashed) with equal equilibrium temperatures, are considered. The growth rate of fluid RWM (solid) is also plotted for comparison. A real mode frequency of $\omega/\omega_A=10^{-3}$ is assumed. The ion gyrofrequency at the plasma center $\omega_{ci}=121\omega_A$.

is mainly current driven, the equilibrium pressure is reasonably high, with $\beta_N=2.847$. The marginal position of an ideal conformal wall is $1.21a$ for the ideal kink stability.

Figure 7 shows the computed kinetic energy following the perturbative approach in MARS-K, together with the fluid energy. All the energy is normalized by the full plasma inertia. The thermal ion temperature is equal to that of the electrons. We consider an ideal situation, where both the plasma rotation frequency and the RWM (complex) frequency vanish, and a situation when the mode growth rate from the fluid calculations is taken into account in the kinetic integrals, $\omega=i\gamma_f$. The kinetic effects of these two approximations on the RWM stability is opposite: the former leads to a negative real δW_k meaning destabilization of the mode, while the latter gives a positive real δW_k meaning stabilization. In both cases, since δW_k is much smaller than δW_f in magnitude, the kinetic correction to the RWM instability is small.

The kinetic correction of the RWM growth rates is shown in Fig. 8, for the two cases from Fig. 7, together with the results from the self-consistent approach. The latter shows a slight stabilization of the mode close to the marginal wall position for ideal kink mode, and a slight destabilization for the more stable RWM. The results of self-consistent computations are different from the perturbative ones. We attribute this difference to the modification of the eigenmode structure in the self-consistent approach, as will be shown later. The degree of kinetic (de-)stabilization of the RWM varies with the plasma equilibria. It has been shown that, in some cases, the mode can be fully stabilized by the drift kinetic effects.[19] Initial MARS-K calculations for a DIII-D[31] plasma, using the perturbative approach, also find full stabilization.

The destabilization effect of the drift resonances on the RWM has been shown in analytical calculations,[27] where the downward shift of the precession drift frequency of ions, due to a finite pressure correction term,[25] is the main cause of this

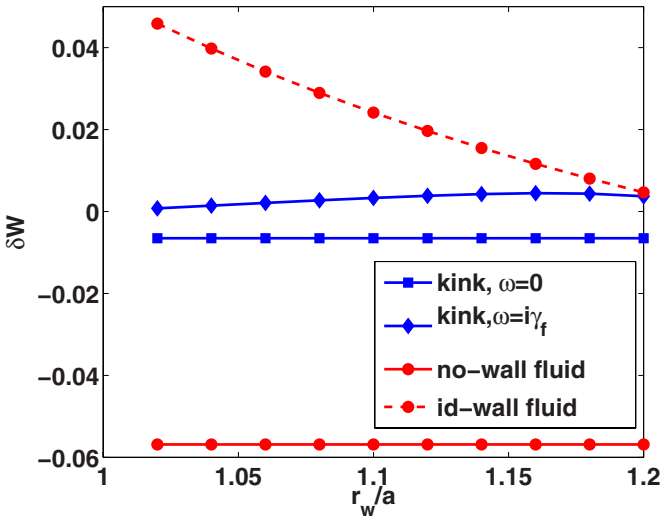

FIG. 7. (Color online) Kinetic and fluid potential energy vs the wall radius, for a Solov'ev equilibrium (23) with parameters (26). The kinetic energy is computed using the eigenfunction of the ideal kink mode without a wall. Both the plasma rotation and the (real) mode frequencies are assumed zero. A comparison is made depending on whether the growth rate of the fluid RWM is included in the kinetic integrals. An ion gyrofrequency at the plasma center $\omega_{ci}=100\omega_A$ is assumed.

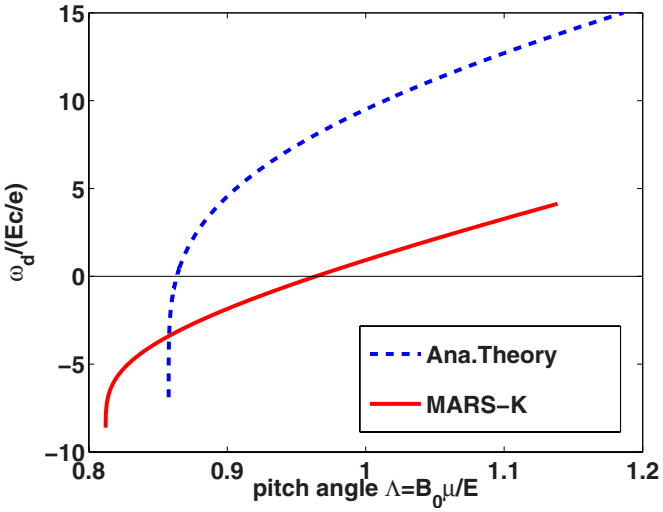

FIG. 9. (Color online) Comparison of the MARS-K computed precession drift frequency, for a Solov'ev equilibrium (23) with parameters (26), with that from the large aspect ratio theory Eq. (25) shows a significant modification by the toroidal effect, as well as the finite pressure effect. The comparison is made at the plasma minor radius $r=0.5a$.

destabilization. A similar shift occurs in the toroidal computations for this equilibrium, as shown by Fig. 9.

The difference in the results between the perturbative and nonperturbative approaches is partly explained by the modification of the eigenmode structures due to the kinetic effects. Figures 10(c), 10(b), and 10(c) compare the normal displacement of the plasma for the ideal kink mode, which is used to compute δW_k in the perturbative approach, with the eigenfunction of the fluid RWM, as well as that from the nonperturbative approach. Both the wall eddy currents outside the plasma and the particle resonances within the plasma contribute to the modification of the ideal kink structure. The kinetic effects generally have an effect of localizing the plasma displacement at larger radii. Since the eigenstructure of the ideal kink without a wall is rather different from the true kinetic eigenfunction, a significant difference in predicting the RWM stability can be expected between the nonperturbative approach and the perturbative approach using the no-wall kink eigenfunction. A better way is to use the eigenfunction of the marginally stable ideal kink (with an ideal wall),[19] which is normally close to that of the fluid RWM. By using the eigenfunction of the fluid RWM as shown in Fig. 10(b), we find that the value of δW_k is reduced by about 30% compared with that from no-wall ideal kink eigenfunction.

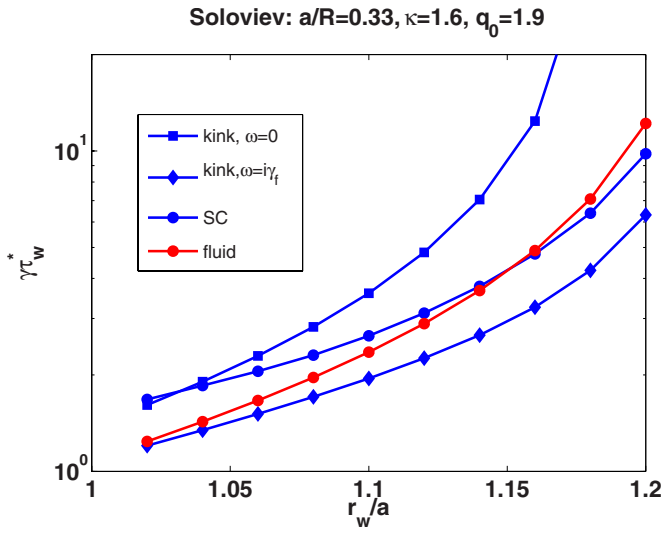

FIG. 8. (Color online) Comparison of the RWM growth rate vs the wall radius r_w under various assumptions, for a Solov'ev equilibrium (23) with parameters (26). The eigenfunction of the ideal kink mode without a wall is used in the perturbative approaches (labeled "kink"). Results are also shown for the self-consistent (SC) approach. Both the plasma rotation and the (real) mode frequencies vanish. An ion gyrofrequency at the plasma center $\omega_{ci}=100\omega_A$ is assumed.

Figures 11(a)–11(c) display the perpendicular component of the perturbed kinetic pressure from two perturbative (a, b) and one self-consistent calculation (c). One observation is that the kinetic integrals tend to generate a richer mode spectrum for $\delta p_\perp$, compared with that for the plasma displacement. Specifically, the higher number poloidal harmonics $m=5,6$ become dominant in these cases. This effect does not appear strongly for the parallel component of the kinetic pressure perturbation. Case (a) presents a peculiar feature of $\delta p_\perp$, which does not vanish towards the plasma edge, despite the fact that the equilibrium pressure vanishes at the plasma edge. It can be analytically shown that this is due to an exact cancellation of the equilibrium pressure in the kinetic integrals, in the absence of the plasma flow and the mode (complex) frequency. This cancellation disappears as soon as a finite plasma flow, or mode frequency, or collisionality is present at the plasma edge. Case (b) presents the result when the fluid growth rate is included in the kinetic integral for the perturbative approach (see Fig. 8). In the nonperturbative calculations, due to the kinetic modification of the mode eigenfunction, the perturbed kinetic pressure also tends to shrink towards the plasma edge. At the same time, the outer

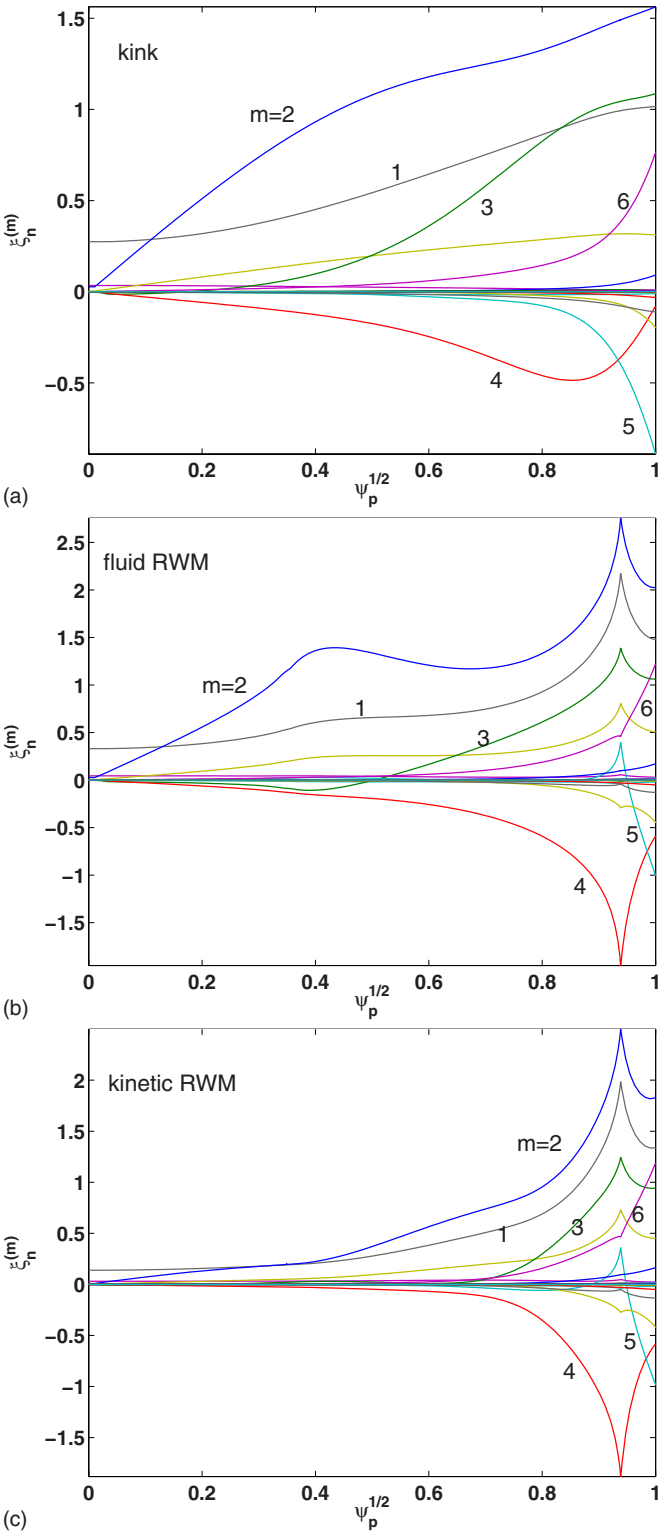

FIG. 10. (Color online) Poloidal Fourier harmonics of the normal displacement for (a) ideal kink mode without wall, (b) fluid RWM, and (c) kinetic RWM from self-consistent calculations, with the wall minor radius $r_w = 1.1a$, for a Solov'ev equilibrium (23) with parameters (26). An equal-arc coordinate system is used. No plasma rotation is assumed.

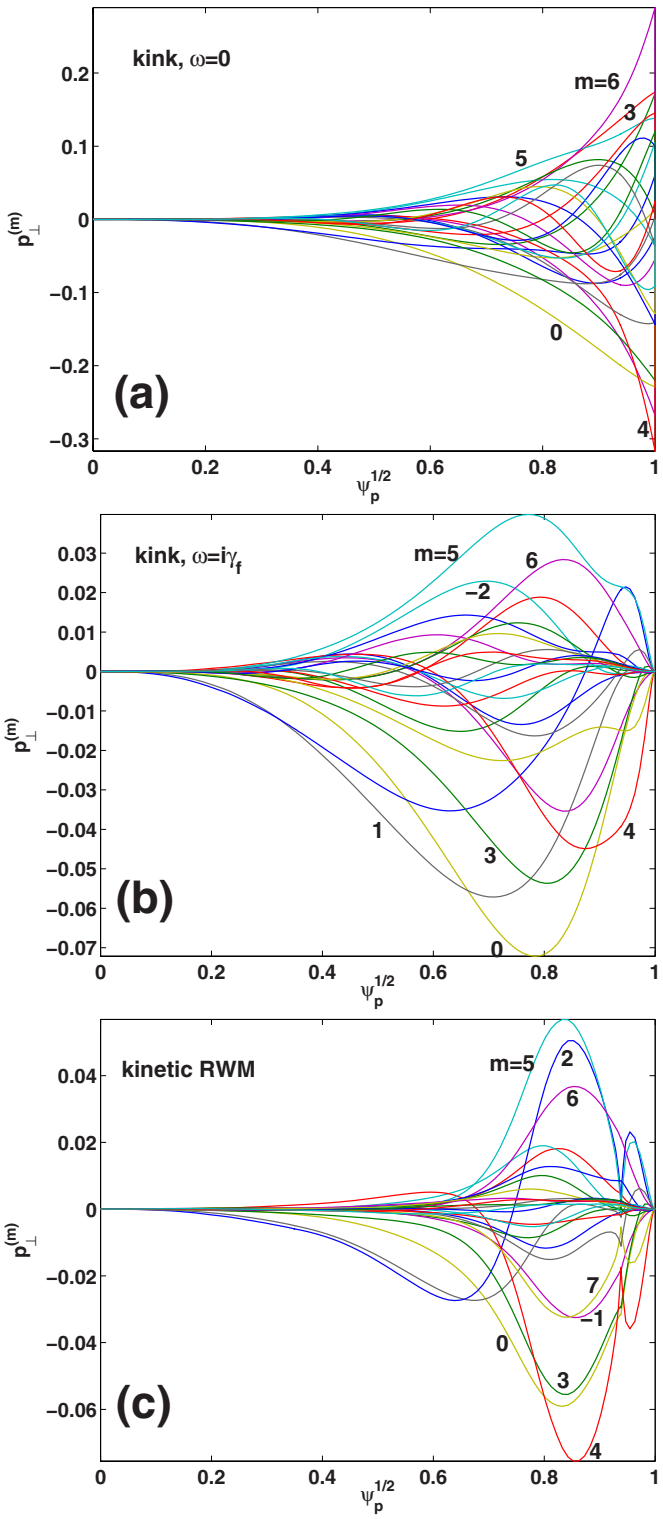

FIG. 11. (Color online) Poloidal Fourier harmonics of the perturbed perpendicular kinetic pressure, computed from (a) perturbative approach assuming vanishing mode frequency and growth rate in the kinetic integrals, (b) perturbative approach assuming vanishing mode frequency and fluid RWM growth rate, and (c) self-consistent approach, for a Solov'ev equilibrium (23) with parameters (26). The wall minor radius is $r_w = 1.1a$. No plasma rotation is assumed.

rational surface at $q=3$ tries to separate the pressure perturbation into two regions.

Figures 12 compare the two-dimensional plots of $\mathrm{Re}(\delta p_\perp)$ at a given toroidal angle. The pressure perturbation patterns are different between perturbative and nonperturbative calculations. The up-down symmetry is well exhibited at no plasma rotation.

Following the perturbative approach, Fig. 13 scans the kinetic potential energy over the real mode frequency (or

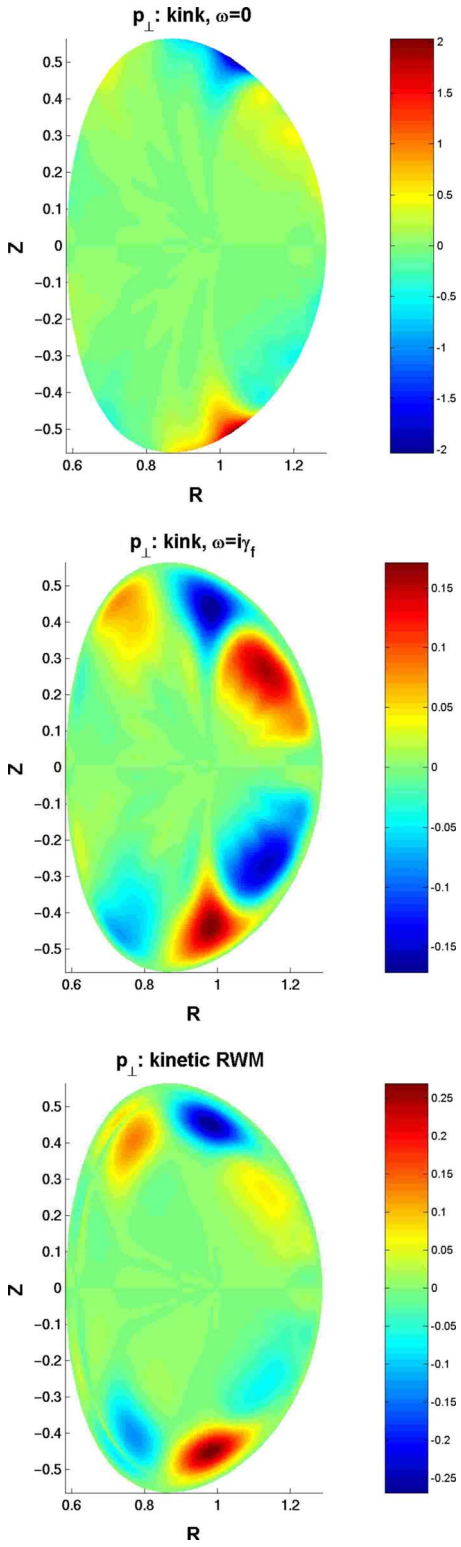

FIG. 12. (Color online) Two-dimensional plot of the perturbed perpendicular kinetic pressure, computed from (a) perturbative approach assuming vanishing mode frequency and growth rate in the kinetic integrals, (b) perturbative approach assuming vanishing mode frequency and fluid RWM growth rate, and (c) self-consistent approach, for a Solov'ev equilibrium (23) with parameters (26). Shown is the real part of the pressure perturbation on a selected toroidal plane. The wall minor radius is $r_w=1.1a$. No plasma rotation is assumed.

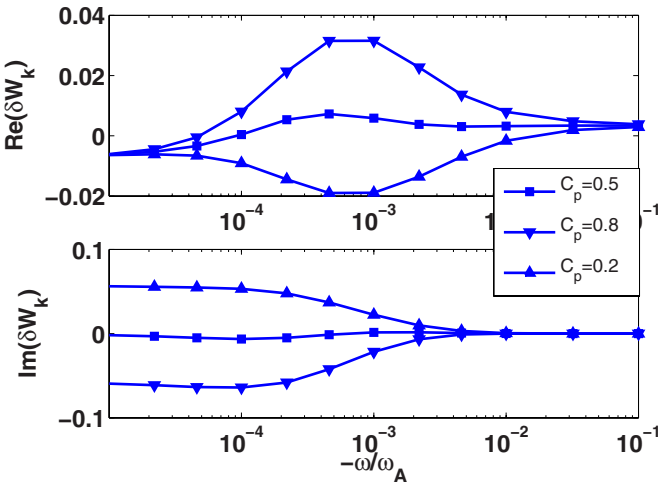

FIG. 13. (Color online) Kinetic energy due to precession drift resonances of thermal trapped particles, vs the mode frequency, for a Solov'ev equilibrium (23) with parameters (26). Results are shown for the perturbative approach with various ratios of ion-electron pressures.

equivalently, over the plasma rotation frequency with a uniform rotation profile if we assume that the plasma rotation does not affect the ideal kink mode). We notice that for $C_p \gtrsim 0.5$, the destabilizing region [negative $\mathrm{Re}(\delta W_k)$] at small mode frequency, as already shown in Fig. 7, smoothly transits to the stabilizing region at higher mode frequency (or plasma rotation frequency). The peak stabilization (for $C_p \gtrsim 0.5$) occurs at the frequency around $5-10\times 10^{-4}\omega_A$, which roughly corresponds to the diamagnetic frequency. In a plasma with significantly unequal temperatures between thermal ions and electrons, the imaginary part of the kinetic energy can be large, and contributes to the stabilization of the RWM at very small mode frequencies. This effect is shown in Fig. 14, where we plot the growth rate of the RWM versus the mode frequency. A complete stabilization of the mode is achieved for both $C_p=0.2$ and 0.8, at the mode frequency below $10^{-3}\omega_A$.

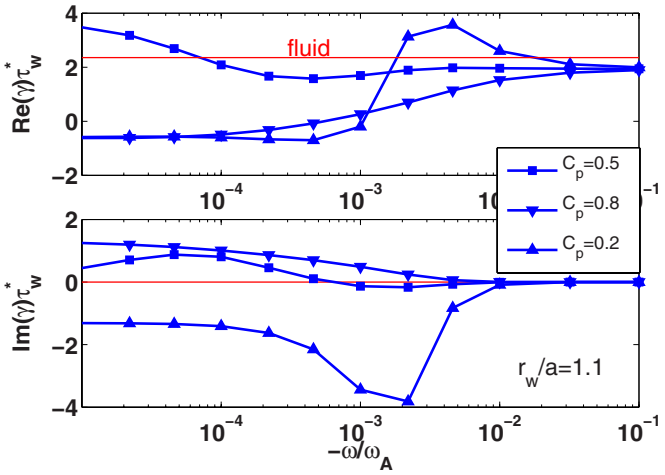

FIG. 14. (Color online) Kinetic modification of the RWM growth rate due to precession drift resonances of thermal trapped particles, vs the mode frequency, for a Solov'ev equilibrium (23) with parameters (26). Results are shown for the perturbative approach with various ratios of ion-electron pressures. The wall radius is $r_w=1.1a$.

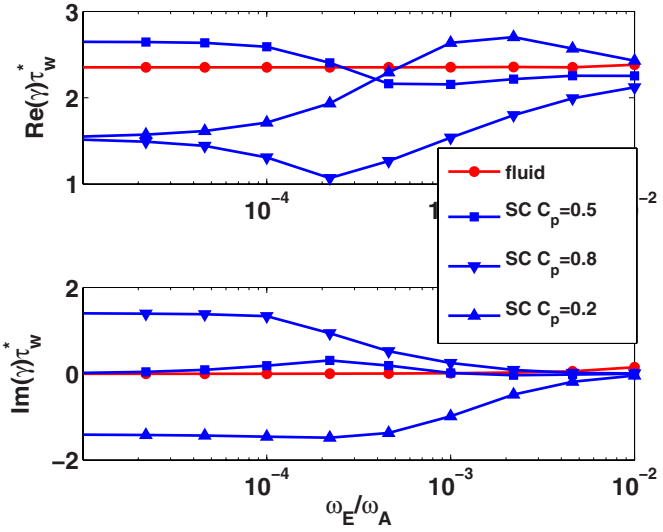

FIG. 15. (Color online) Kinetic modification of the RWM growth rate due to precession drift resonances of thermal trapped particles, vs the plasma rotation frequency, for a Solov'ev equilibrium (23) with parameters (26). The self-consistent approach is considered for various ratios of ion-electron pressures. The growth rate of fluid RWM is also plotted for comparison. The wall radius position is $r_w=1.1a$. A uniform plasma rotation profile is assumed.

Following the nonperturbative approach, Fig. 15 scans the growth rate of the kinetic RWM over the plasma rotation frequency, assuming a uniform rotation profile. For comparison, the growth rate of fluid RWM is also plotted, which is subject to MHD continuum (Alfvén and sound waves) damping in these calculations. For this plasma, within the fluid framework, a toroidal rotation frequency of up to $1\%\omega_A$ does not result in a noticeable modification of the RWM growth rate. The kinetic resonances with magnetic drifts of trapped particles, however, do stabilize or destabilize the mode, depending on the rotation frequency and the ion-electron temperature ratio. The results generally resemble that of the perturbative approach (Fig. 14), with the difference that the kinetic RWM is less stabilized according to the self-consistent approach; in particular, for a rotation frequency range between 0 and $10^{-3}\omega_A$ and $C_p=0.8$ or 0.2, the perturbative approach predicts complete stabilization, whilst the self-consistent computations still yield positive growth rates.

The fact that the nonperturbative approach predicts less stabilization of the kinetic RWM than the perturbative approach, can be attributed to the kinetic modification of the eigenfunction, as shown before, as well as to the self-consistent inclusion of the mode growth rate in the kinetic integrals, resulting in a nonlinear eigenvalue problem. We go through a qualitative analysis here showing this effect.

Following Eq. (1), and introducing a new quantity $\hat{\gamma}=\gamma\tau_w^*$, we have

$$\hat{\gamma}=-\frac{\delta W_\infty+\delta W_k}{\delta W_b+\delta W_k}=\frac{1-\delta W_k/(-\delta W_\infty)}{\delta W_b/(-\delta W_\infty)+\delta W_k/(-\delta W_\infty)}$$

$$=\frac{1-C}{\hat{\gamma}_0^{-1}+C}\equiv F(C), \tag{27}$$

where we have denoted the normalized growth rate of fluid RWM by $\hat{\gamma}_0$, and introduced a normalized kinetic energy $C=\delta W_k/(-\delta W_\infty)$. Examining the resonance condition (15) for trapped particles (i.e., $\alpha=l=0$), and neglecting the plasma rotation, we can assume that the factor C has the following structure:

$$C(\gamma)=c\left[\frac{\omega_{*i}-i\gamma}{\omega_{di}-i\gamma}+\frac{\omega_{*e}-i\gamma}{\omega_{de}-i\gamma}\right],$$

where c is a constant, and $\omega_{*i,e}$ and $\omega_{di,e}$ represent "lumped" diamagnetic and magnetic drift frequencies, respectively, for ions and electrons. For a case of equal temperature between ions and electrons ($C_p=0.5$), we can assume $\omega_{*i}=-\omega_{*e}=\omega_*$ and $\omega_{di}=-\omega_{de}=\omega_d$. Further introducing a normalization $\hat{\omega}_*=\omega_*\tau_w^*$, $\hat{\omega}_d=\omega_d\tau_w^*$, we rewrite

$$C(\hat{\gamma})=2c\frac{\hat{\omega}_*\hat{\omega}_d+\hat{\gamma}^2}{\hat{\omega}_d^2+\hat{\gamma}^2}.$$

Note that for $c>0, \hat{\omega}_*>\hat{\omega}_d>0$, which is normally the case, C is a positive and monotonically decreasing function of $\hat{\gamma}$.

In the perturbative approach, normally we assume $\hat{\gamma}=0$ in the kinetic integrals; i.e., $C(0)=C_1=2c\hat{\omega}_*/\hat{\omega}_d$. In the self-consistent approach, we have to solve a nonlinear dispersion relation (27) to find $\hat{\gamma}=\hat{\gamma}_2$. However, independent of the solution, we know that $C(\hat{\gamma}_2)=C_2<C_1$. Thanks to the monotonic decreasing behavior of the function $F(C)$, we obtain $\hat{\gamma}_2>\hat{\gamma}_1$, i.e., the growth rate of self-consistent calculation is always larger than that of the perturbative approach, under the assumptions made in the above derivations. Finally, introducing the growth rate $\hat{\gamma}_3$ from the perturbative approach, where the fluid eigenvalue γ_0 is used in the kinetic integral, we obtain a relation

$$\hat{\gamma}_1<\hat{\gamma}_2<\hat{\gamma}_3<\hat{\gamma}_0.$$

It should be noted that this is not an absolute proof because changes to the eigenfunction structure between the perturbative and self-consistent approaches could affect the conclusion.

V. SUMMARY AND DISCUSSION

We have developed a toroidal kinetic model for the RWM, where the drift kinetic terms are included self-consistently into the ideal MHD equations with plasma flow. This allows us to study the effects of kinetic modification of the mode eigenfunction on the stability of the RWM, and compare the results with the perturbative approach, where the eigenfunction of an ideal kink mode is used to compute the perturbed kinetic energy.

A new version of the MARS code, MARS-K, has been developed and benchmarked against both analytical results and other numerical codes using a perturbative approach.

In the perturbative calculations, we find that the precessional drift kinetic resonances can contribute to either stabilization or destabilization of the RWM, depending on the plasma equilibrium and the toroidal rotation. The destabilization can occur at very small rotation/mode frequency, as a result of the finite pressure correction to the particle preces-

sion drifts. A complete stabilization is possible even for a current-driven RWM, due to a large imaginary part of the kinetic energy, in a plasma with unequal equilibrium temperatures between thermal ions and electrons.

The nonperturbative calculations normally predict less stabilization than the perturbative ones. We observe a modification of the mode eigenfunction by the kinetic resonances, which pushes the plasma displacement (and the perturbed kinetic pressure) towards the plasma edge. This modification can be large in some cases. Self-consistent inclusion of the mode growth rate in the kinetic integrals can also contribute to the destabilization effect compared with the perturbative approach.

In a future study, we will apply the MARS-K code to experimental plasma configurations, as well as to the ITER steady state scenarios.

ACKNOWLEDGMENTS

Y.Q.L. thanks Dr. C. G. Gimblett and Dr. R. J. Hastie from UKAEA Culham and Professor J. Weiland from Chalmers University of Technology for many fruitful discussions during this work.

This work was partly funded jointly by the United Kingdom Engineering and Physical Sciences Research Council and by the European Communities under the contract of Association between EURATOM and UKAEA. The views and opinions expressed herein do not necessarily reflect those of the European Commission. This work was also supported by the U.S. Department of Energy under Contract No. DE-FG03-956ER54309.

[1] C. Kessel, J. Manickam, G. Rewoldt, and W. M. Tang, Phys. Rev. Lett. **72**, 1212 (1994).
[2] R. Aymar, P. Barabaschi, and Y. Shimomura, Plasma Phys. Controlled Fusion **44**, 519 (2002).
[3] Y. Liu, A. Bondeson, Y. Gribov, and A. Polevoi, Nucl. Fusion **44**, 232 (2004).
[4] H. Reimerdes, A. M. Garofalo, G. L. Jackson, M. Okabayashi, E. J. Strait, M. S. Chu, Y. In, R. J. La Haye, M. J. Lanctot, Y. Q. Liu, G. A. Navratil, W. M. Solomon, H. Takahashi, and R. J. Groebner, Phys. Rev. Lett. **98**, 055001 (2007).
[5] E. J. Strait, A. M. Garofalo, G. L. Jackson, M. Okabayashi, H. Reimerdes, M. S. Chu, R. Fitzpatrick, R. J. Groebner, Y. In, R. J. LaHaye, M. J. Lanctot, Y. Q. Liu, G. A. Navratil, W. M. Solomon, H. Takahashi, and the DIII-D Team, Phys. Plasmas **14**, 056101 (2007).
[6] A. Bondeson and D. J. Ward, Phys. Rev. Lett. **72**, 2709 (1994).
[7] J. Finn, Phys. Plasmas **2**, 198 (1995).
[8] R. Betti, Phys. Rev. Lett. **74**, 2949 (1995).
[9] D. Gregoratto, A. Bondeson, M. S. Chu, and A. M. Garofalo, Plasma Phys. Controlled Fusion **43**, 1425 (2001).
[10] L.-J. Zheng, M. Kotschenreuther, and M. S. Chu, Phys. Rev. Lett. **95**, 255003 (2005).
[11] C. G. Gimblett and R. J. Hastie, Phys. Plasmas **7**, 258 (2000).
[12] M. S. Chu, J. M. Greene, T. H. Jensen, R. L. Miller, A. Bondeson, R. W. Johnson, and M. E. Mauel, Phys. Plasmas **2**, 2236 (1995).
[13] R. J. La Haye, A. Bondeson, M. S. Chu, A. M. Garofalo, Y. Q. Liu, G. A. Navratil, M. Okabayashi, H. Reimerdes, and E. J. Strait, Nucl. Fusion **44**, 1197 (2004).
[14] Y. Q. Liu, A. Bondeson, M. S. Chu, J.-Y. Favez, Y. Gribov, M. Gryaznevich, T. C. Hender, D. F. Howell, R. J. La Haye, and J. B. Lister, Nucl. Fusion **45**, 1131 (2005).
[15] Y. Liu, M. S. Chu, A. M. Garofalo, Y. Gribov, M. Gryaznevich, T. C. Hender, D. F. Howell, R. J. La Haye, M. Okabayashi, S. D. Pinches, H. Reimerdes, P. de Vries, and EFDA-JET Contributors, Phys. Plasmas **13**, 056120 (2006).
[16] A. Bondeson and M. S. Chu, Phys. Plasmas **3**, 3013 (1996).
[17] Y. Q. Liu, A. Bondeson, C. M. Fransson, B. Lennartson, and C. Breitholtz, Phys. Plasmas **7**, 3681 (2000).
[18] B. Hu and R. Betti, Phys. Rev. Lett. **93**, 105002 (2004).
[19] B. Hu, R. Betti, and J. Manickam, Phys. Plasmas **12**, 057301 (2005).
[20] S. W. Haney and J. P. Freidberg, Phys. Fluids B **1**, 1637 (1989).
[21] T. M. Antonsen and Y. C. Lee, Phys. Fluids **25**, 132 (1982).
[22] F. Porcelli, R. Stankiewicz, W. Kerner, and H. L. Berk, Phys. Plasmas **1**, 470 (1994).
[23] L. S. Solov'ev, in Reviews of Plasma Physics Vol 6, edited by M. A. Leontovich (Consultants Bureau, New York, 1975), p. 257.
[24] B. B. Kadomtsev and O. P. Pogutse, Sov. Phys. JETP **24**, 1172 (1967).
[25] J. W. Connor, R. J. Hastie, and T. J. Martin, Nucl. Fusion **23**, 1702 (1983).
[26] M. D. Kruskal and C. R. Oberman, Phys. Fluids **1**, 275 (1958).
[27] Y. Liu, M. S. Chu, C. G. Gimblett, and R. J. Hastie, Phys. Plasmas **15**, 092505 (2008).
[28] I. T. Chapman, M. P. Gryaznevich, C. G. Gimblett, T. C. Hender, D. F. Howell, Y. Q. Liu, S. D. Pinches, and JET EFDA Contributors, "Kinetic effects on the resistive wall mode," Plasma Phys. Controlled Fusion (unpublished).
[29] A. B. Mikhailovskii, G. T. A. Huysmans, S. E. Sharapov, and W. O. Kerner, Plasma Phys. Rep. **23**, 844 (1997).
[30] S. D. Pinches, L. C. Appel, J. Candy, S. E. Sharapov, H. L. Berk, D. Borba, B. N. Breizman, T. C. Hender, K. I. Hopcraft, G. T. A. Huysmans, and W. Kerner, Comput. Phys. Commun. **111**, 133 (1998).
[31] J. L. Luxon, Nucl. Fusion **42**, 614 (2002).